# SENSITIVITY ANALYSIS OF COAL GASIFICATION IN TWO-STAGE ENTRAINED-FLOW GASIFIER: SYNGAS AND CARBON CONVERSION PREDICTION

M. S. Alam[1, 2], A. T. Wijayanta[3], K. Nakaso[2], J. Fukai[2, *]

## ABSTRACT

The energy production from coal-fired power plant is increasing day by day, which result in increased $CO_2$ emission from the existing power plant. However, $CO_2$ emission from coal gasification can be reduced if an efficient $CO_2/O_2/N_2$ coal gasification is implemented in IGCC system. Numerical simulations of coal gasification under $CO_2/O_2/N_2$ gasification condition are carried out with the aim of describing the effects of model parameters, char reaction rates, operating conditions and heat losses to increase the syngas heating value and carbon conversion in a two stage entrained flow coal gasification process. The Eulerian–Lagrangian approach is applied to solve the Navier–Stokes equation and the particle dynamics. Finite rate/eddy dissipation model is used to calculate the rate of nine homogeneous gas-to-gas phase reactions. While only finite rate is used for the heterogeneous solid-to-gas phase reactions. It is found that the carbon conversions of combustor coal lie in the ranges from 97 wt% to 99 wt% for most of the calculated conditions. On the other hand, the carbon conversion of reductor coals varies from 45 wt% to 57 wt%. A noticeable change is obtained when the gasification occurs under a high-temperature condition. Remarkable outlet results of about 32 wt% CO, 0.58 wt% $H_2$ and 89 wt% overall carbon conversion are predicted if a high temperature of 1673K is maintained in the reductor. On the other hand, a reduced soot concentration is predicted if the $O_2$ concentration and/or the reductor gas temperature increase(s) in the gasifier.

**Keywords:** *Sensitivity Analysis, Two-stage Gasifier, Syngas Heating Value, $CO_2$-blown*

## INTRODUCTION

Global energy consumption in 2030 is predicted to increase 1.4 times that in 2007, where about half of the increase will be contributed by Asia. It is also predicted that remaining years of exploitable global energy resources in sequences are 122 years for coal, 100 years for uranium, 60 years for natural gas, and 42 years for oil [1]. Because of more exploitable coal resource compared to other resources, it is expected that coal will continue to play a significant role in meeting the future energy demand. However, due to use of fossil fuel mainly coal to generate power, a large amount of $CO_2$ is discharged from conventional coal fired power plant, which is deemed as one of the major causes of global warming. Although technologies for employing renewable energy such as solar, wind, ocean, hydro, and biomass have been developed, the advantage of utilizing fossil fuels (mainly coal) for providing the most affordable electrical energy cannot be replaced overnight by any other technologies today [2]. However, clean coal technologies need to be implemented in the power sector in an effort to meet the environmental targets.

A number of research programs are now under way all over the world to test and develop efficient and economical production of high heating value gas from coal. However, to date, there has been no published work investigating the coal gasification under $CO_2/O_2/N_2$ atmosphere in two stage entrained flow gasifier. Chen et al. [3-4] performed a series of numerical simulation for a 200 T/D two-stage air blown entrained flow gasifier under various operating conditions such as heterogeneous reaction rate, particle size, and coal partitioning to the two stages. They reported that the carbon conversion decreases when the pre-exponential factor for the char reaction rates and average coal particle size are decreased. The carbon conversion and the syngas heating value were predicted to change very little with the coal partitioning. Silaen and Wang [5-7] conducted numerical simulation of the coal gasification process in two stage entrained flow gasifier to investigate the effects of several

parameters on gasification performance. The air-blown operation yielded poor fuel conversion efficiency and the lowest syngas heating value due to air dilution. The effect of wall cooling has been shown insignificant on the exit gas composition and heating value. The case with coal distribution with 75% (combustor) vs. 25% (reductor) showed better fuel conversion efficiency than that with 50% vs. 50% . They also revealed that the horizontal injection direction gave the best gasifier performance.

In our previous study [8], numerical simulations of coal gasification were conducted with the aim of describing the coal gasification behaviors under $CO_2/O_2/N_2$ atmosphere in an effort to increase the syngas production. It was predicted that carbon conversion gradually increased with an increased in $O_2$ ratio, while producing syngas with a low heating value beyond a certain limit of $O_2$ ratio. In contrast, an increase in $CO_2$ concentration in the gasifier increased heating value of product syngas. This paper would lead to sensitivity analysis on coal gasification under $CO_2$-blown gasification condition to increase carbon conversion and syngas production. Sensitivity analysis was the study of the variation in the predicted results when a component of the model or an input to the model is changed. In gasification the predictions made by a model can be a number of different variables including soot formation, carbon conversion, syngas composition and exit gas temperature. Therefore, the main objectives of this work are to investigate the uncertainty of model parameters, effects of char reaction rates, effects of operating conditions, effects of heat losses etc. in an effort to increase the syngas heating value and carbon conversion in coal gasification. The heating value of product syngas is considered to be the sum of energy release burning the component gas as follows:

$$Heating\ \ value = Heating\ \ value\ \ of\ \ CO \times Y_{CO} + Heating\ \ value\ \ of\ \ H_2 \times Y_{H_2} \qquad (1)$$

where heating value of CO and $H_2$ are considered as 12372 and 141790 kJ/kg [9], respectively. $CO_2$ and $H_2O$ are non combustible gases and therefore make no energy contribution.

## NUMERICAL METHODS

The coal gasifier (Figure 1) considered here consists of a combustor stage and a reductor stage [10]. It has two levels of injectors that are positioned axisymmetrically at combustor and reductor stage. The combustor injectors are placed similar to a tangential firing system to create swirling flow inside the gasifier. The reductor injectors are directed towards the center of the gasifier. All governing equations and related auxiliary equations are summarized in Table 1. Details of the governing equations and reaction models can be found in the previous report [8]. Uniform distributions of inlet mass flow rate and temperature are given for all inlet boundary surfaces. The walls are assumed as stationary and smooth with no slip condition. A constant wall heat flux is assigned for the wall surfaces. The boundary condition of the discrete phase at walls is assigned as "reflect", which means the discrete phase elastically rebound off once reaching the wall. At the outlet, the discrete phase exits the computational domain.
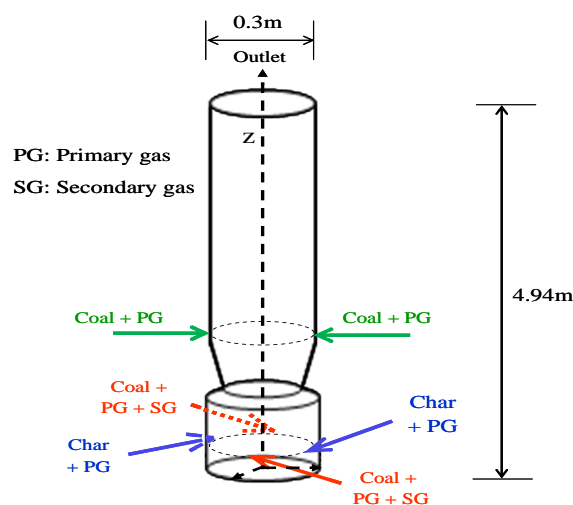


**Figure 1.** Schematic of computational model adopted from CRIEPI [10]

**Table 1.** Governing equations for the gas and particle phases

| | |
|---|---|
| Equations for the conservation of mass, momentum, energy and species:<br>Continuity: $\nabla \cdot (\rho \vec{v}) = S_m$ | (2) |
| Momentum: $\nabla \cdot (\rho \vec{v} \vec{v}) = -\nabla p + \nabla \cdot (\overline{\overline{\tau}}) + \rho \vec{g} + \vec{F}$ | (3) |
| Energy: $\nabla \cdot (\vec{v}(\rho E + p)) = -\nabla \cdot \left( \sum_i H_i J_i \right) + I_{rad} + S_{h,reac}$ | (4) |
| Species: $\nabla \cdot (\rho \vec{v} Y_i) = -\nabla \cdot \vec{J}_i + R_i + S_i$ | (5) |
| Transport equation for standard $k$–$\varepsilon$ model:<br>$\dfrac{\partial}{\partial x_i}(\rho k u_i) = \dfrac{\partial}{\partial x_j}\left[ \left( \mu + \dfrac{\mu_t}{\sigma_k} \right) \dfrac{\partial k}{\partial x_j} \right] + G_k - \rho \varepsilon$ | (6) |
| $\dfrac{\partial}{\partial x_i}(\rho \varepsilon u_i) = \dfrac{\partial}{\partial x_j}\left[ \left( \mu + \dfrac{\mu_t}{\sigma_\varepsilon} \right) \dfrac{\partial \varepsilon}{\partial x_j} \right] + C_{1\varepsilon} G_k \dfrac{\varepsilon}{k} - C_{2\varepsilon} \rho \dfrac{\varepsilon^2}{k}$ | (7) |
| Radiative transfer equation (Discrete Ordinates):<br>$\dfrac{dI_{rad}(\vec{r}, \vec{s})}{ds} = -(a + a_p + \sigma_p) I_{rad}(\vec{r}, \vec{s}) + E_p + a\varphi^2 \dfrac{\sigma T^4}{\pi} + \dfrac{\sigma_s}{4\pi} \int_0^{4\pi} I_{rad}(\vec{r}, \vec{s}') \Phi(\vec{s}.\vec{s}') d\Omega$ | (8) |
| Continuity and momentum equations of particles:<br>$dm_p / dt = \dot{m}$ | (9) |
| $\dfrac{du_p}{dt} = F_D(u - u_p) + \dfrac{g(\rho_p - \rho)}{\rho_p}$ | (10) |
| Energy balance equation for devolatilization:<br>$m_p C_p (dT_p / dt) = hA_p(T - T_p) + (dm_p / dt)L + A_p \varepsilon_p \sigma(\theta_R^4 - T_p^4)$ | (11) |
| Energy balance equation for surface reactions:<br>$m_p C_p \dfrac{dT_p}{dt} = hA_p(T - T_p) - f_h\left( \dfrac{dm_p}{dt} \right)\Delta H + A_p \varepsilon_p \sigma(\theta_R^4 - T_p^4)$ | (12) |
| Kinetic equation for coal devolatilization (Kobayashi model):<br>$\dfrac{m_p(t)}{(1 - f_{w,0})m_{p,0} - m_a} = \int_0^t (\alpha_1 k_{kin,1} + \alpha_2 k_{kin,2}) \exp\left( -\int_0^t (k_{kin,1} + k_{kin,2}) dt \right) dt$ | (13) |
| Reaction rate equation for gas phase reactions (finite rate and the eddy dissipation models):<br>$\hat{R}_{i,k}^{(A)} = (\upsilon_{i,k}'' - \upsilon_{i,k}')\left( k_{kin,f,k} \prod_{i=1}^I [X_i]^{\eta_{i,k}'} - k_{kin,b,k} \prod_{i=1}^I [X_i]^{\eta_{i,k}''} \right)$ | (14) |
| $\hat{R}_{i,k}^{(R)} = v_{i,k}' M_i A_R \rho \left( \dfrac{\varepsilon}{k} \right) \min_R \left( \dfrac{Y_R}{v_{R,k}' M_R} \right)$ | (15) |
| $\hat{R}_{i,k}^{(P)} = v_{i,k}' M_i A_R B_P \rho \left( \dfrac{\varepsilon}{k} \right)\left( \dfrac{\sum_P Y_P}{\sum_j^N v_{j,k}'' M_j} \right)$ | (16) |
| Reaction rate equation for gas-solid reactions (Finite rate model):<br>$\overline{R}_k = A_p \eta_k Y_{carbon} \tilde{R}_k$ | (17) |
| $\tilde{R}_k = k_{kin,k}\left( p_{i,k} - \tilde{R}_k / D_k \right)^{N_k}$ | (18) |
| Rate equation for kinetic reactions (Arrhenius expression):<br>$k_{kin} = A_f \exp^{-(E_{ac} / RT_p)}$ | (19) |

To solve the governing equations used in the simulation, the overall gas-particle coupling follows an iterative solution procedure using Ansys Fluent 12 [11]. The implicit time integration method is used to solve instantaneous mass, momentum and energy equations of discrete particles to obtain a converged steady-state solution. The discretization of the equations governing the gas phase is based on the finite volume method using a staggered grid and solved by the SIMPLE algorithm for pressure–velocity coupling. Solution control was achieved through under relaxation, which helped to stabilize the convergence behavior of the outer nonlinear iterations in the system of discretized equations. First order upwind scheme is used for spatial discretization of the convective terms. Iterations are repeated until convergence is reached for both phases.

Making a uniform mesh with a small mesh size (2mm or less) will significantly increase the computational time. A three dimensional mesh consisting of 247,818 computational cells is used with the small cell size being around 2 mm and the largest one around 10 mm. The near wall $y^+$ value is 250, which is appropriate ($30 > y^+ > 300$) to apply the standard wall functions in the standard $k$-$\varepsilon$ turbulence model.

## CALCULATION CONDITIONS

A bituminous type CV coal (Coal Valley, Canada) is used to conduct the simulation of coal gasification. The proximate and ultimate analyses of coal are given in Table 2. The particle size distributions with a mean diameter of 60 μm are assumed (see Figure 6). The coal flow rates for combustor and reductor are set to 40 kg/h and 60 kg/h, respectively. The gas flow rates are adjusted in such a way that the inlet $O_2$ ratio, $O_2$ concentration and $CO_2$ concentration become 0.528, 23 wt% and 23 wt%, respectively. Kinetic parameters for gas and surface phase reactions are summarized in Table 3. The calculation conditions for case 1 (standard case) are listed in Table 4.

**Table 2.** Analyses of coal (CV coal) [12]

| Parameters | CV coal (Canada) |
|---|---|
| Proximate analyses(air dried) | |
|   Moisture [wt%] | 6.22 |
|   Fixed carbon [wt%] | 49.00 |
|   Volatile matter [wt%] | 34.50 |
|   Ash [wt%] | 10.28 |
| Ultimate analyses(dry base) | |
|   C [wt%] | 69.90 |
|   H [wt%] | 4.30 |
|   O [wt%] | 13.70 |
|   N [wt%] | 1.07 |
| High heating value [MJ/kg] | 26.40 |
| Low heating value [MJ/kg] | 26.02 |

## RESULTS AND DISCUSSION

### Effect of model parameters

In the modeling of coal gasification, there are many uncertain parameters used in the calculation. It is very difficult to get exact value of various model parameters for the specific problem especially in coal gasification. Use of uncertain values of model parameters may cause large difference between calculations and experiments.

**Table 3.** Kinetic parameters for gas and surface phase reactions for case 1

| | $A_f$ [consistent unit] | $E_{ac}$ [J/kmol] | Reference (s) |
|---|---|---|---|
| Devolatilization Step 1: Coal $\rightarrow$ Volatile$_1$ + Char$_1$ | | | |
| | $2.00 \times 10^5$ | $1.05 \times 10^8$ | [13] |
| Devolatilization Step 2: Coal $\rightarrow$ Volatile$_2$ + Char$_2$ | | | |
| | $1.30 \times 10^7$ | $1.67 \times 10^8$ | [13] |
| (R1) $C_{\alpha 1}H_{\alpha 2}O_{\alpha 3}N_{\alpha 4} \rightarrow \beta_1 CO + \beta_2 CO_2 + \beta_3 H_2 + \beta_4 CH_4 + \beta_5 H_2O + \beta_6 C_6H_6 + \beta_7 N_2$ | | | |
| $K_{kin,1}$ | $3.09 \times 10^8$ | $1.67 \times 10^8$ | [14] |
| (R2) $CO + \frac{1}{2}O_2 \rightarrow CO_2$ | | | |
| $K_{kin,2}$ | $2.20 \times 10^{12}$ | $1.67 \times 10^8$ | [7, 15] |
| (R3) $CO + H_2O \leftrightarrow CO_2 + H_2$ | | | |
| $K_{kin,3f}$ | $2.75 \times 10^2$ | $8.38 \times 10^7$ | [7, 15] |
| $K_{kin,3b}$ | $2.65 \times 10^{-2}$ | $3.96 \times 10^3$ | [7, 15] |
| (R4) $CH_4 + H_2O \leftrightarrow CO + 3H_2$ | | | |
| $K_{kin,4f}$ | $4.40 \times 10^{11}$ | $1.68 \times 10^8$ | [7, 15] |
| $K_{kin,4b}$ | $5.12 \times 10^{-14}$ | $2.73 \times 10^4$ | [7, 15] |
| (R5) $CH_4 + \frac{1}{2}O_2 \rightarrow CO + 2H_2$ | | | |
| $K_{kin,5}$ | $3.00 \times 10^8$ | $1.26 \times 10^8$ | [7, 15] |
| (R6) $H_2 + \frac{1}{2}O_2 \rightarrow H_2O$ | | | |
| $K_{kin,6}$ | $6.80 \times 10^{15}$ | $1.68 \times 10^8$ | [7, 15] |
| (R7) $4C_6H_6 \rightarrow C_{24}H_{12} + 6H_2$ | | | |
| $K_{kin,7}$ | $1.50 \times 10^{10}$ | $4.70 \times 10^5$ | [16, 17] |
| (R8) $C_6H_6 + 4.5O_2 \rightarrow 6CO + 3H_2O$ | | | |
| $K_{kin,8}$ | $2.00 \times 10^9$ | $3.10 \times 10^7$ | [18] |
| (R9) $C_{24}H_{12} + 15O_2 \rightarrow 24CO + 6H_2O$ | | | |
| $K_{kin,9}$ | $2.00 \times 10^9$ | $3.10 \times 10^7$ | [18] |
| (R10) $C + \frac{1}{2}O_2 \rightarrow CO$ | | | |
| $K_{kin,10}$ | 0.0520 | $1.30 \times 10^8$ | [3, 7, 15] |
| (R11) $C + CO_2 \rightarrow 2CO$ | | | |
| $K_{kin,11}$ | 0.0732 | $1.62 \times 10^8$ | [3, 7, 15] |
| (R12) $C + H_2O \rightarrow CO + H_2$ | | | |
| $K_{kin,12}$ | 0.0782 | $1.47 \times 10^8$ | [3, 7, 15] |

**Table 4.** Calculation conditions for case 1

| Parameter | Value |
|---|---|
| **Properties of gas & particle/Model constants:** | |
| Thermal conductivity, $k_g$ | 0.0454 W/m·K |
| Viscosity, $\mu$ | $1.72 \times 10^{-5}$ kg/m·s |
| Absorption coefficient, $a$ | 1.5 m$^{-1}$ |
| Scattering coefficient, $\sigma_s$ | 0 m$^{-1}$ |
| Refractive index, $\varphi$ | 1 |
| Mass diffusion coefficient, $D$ | $2.88 \times 10^{-5}$ m$^2$/s |
| Particle density, $\rho_p$ | 1400 kg/m$^3$ |
| Particle specific heat, $C_p$ | 1680 J/kg·K |
| Particle Vaporization temperature, $T_{vap}$ | 400 K |
| Particle emissivity, $\varepsilon_p$ | 0.9 |
| Particle scattering factor, $f_p$ | 0.9 |
| Fraction of heat absorbed by coal particle, $f_h$ | 1.0 |
| Latent heat of water, $L$ | 0 J/kg |
| Turbulent Schmidt number, $Sc_t$ | 0.7 |
| Turbulent model constant, $C_{1\varepsilon}$ | 1.44 |
| Turbulent model constant, $C_{2\varepsilon}$ | 1.92 |
| Turbulent model constant, $C_\mu$ | 0.09 |
| Turbulent Prandtl number for $k$, $\sigma_k$ | 1.0 |
| Turbulent Prandtl number for $\varepsilon$, $\sigma_\varepsilon$ | 1.3 |
| **Operating/Boundary conditions:** | |
| Reductor coal injection pattern | Directly to the center of reactor |
| Particle diameter ranges | 10-70 μm |
| Combustor secondary O$_2$ feed<br>Reductor primary O$_2$ feed | 70.80 kg/h<br>16.28 kg/h |
| Combustor coal inlet<br>Reductor coal inlet | 40 kg/h<br>60 kg/h |
| Heat loss at combustor wall<br>Heat loss at reductor wall | 3000 w/m$^2$<br>2400 w/m$^2$ |

**Table 5.** Calculated results for cases 2-14

| Case | Variable changes | Outlet CO [-] | Outlet H$_2$ [-] | Outlet soot [wt%] | Relative change in syngas heating value with respect to case 1 [%] |
|---|---|---|---|---|---|
| **Effect of model parameters** | | | | | |
| 2 | Latent heat of water, $L$: $0 \rightarrow 3.8 \times 10^5$ J/kg | 16.53 | 0.44 | 1.77 | -0.732 |
| 3 | Fraction of heat absorbed by coal particle, $f_h$: $1.0 \rightarrow 0.5$ | 16.86 | 0.45 | 1.81 | 1.31 |
| 4 | Scattering coefficient, $\sigma_s$: $0 \rightarrow 1.5$ m$^{-1}$ | 17.54 | 0.49 | 1.77 | 6.55 |
| 5 | Absorption coefficient, $a$: $1.5 \rightarrow 3.0$ m$^{-1}$ | 20.10 | 0.53 | 1.82 | 20.44 |
| **Effect of char kinetic rates** | | | | | |
| 6 | Pre-exponential factor for char-O$_2$ reaction rate, $A_f$: $0.052 \rightarrow 0.52$ | 17.85 | 0.43 | 1.82 | 4.81 |
| 7 | Pre-exponential factor for char-CO$_2$ reaction rate, $A_f$: $0.0732 \rightarrow 0.732$ | 18.35 | 0.45 | 1.78 | 8.17 |
| 8 | Pre-exponential factor for char-H$_2$O reaction rate, $A_f$: $0.0782 \rightarrow 0.782$ | 19.05 | 0.63 | 1.85 | 20.88 |
| **Effect of operating conditions** | | | | | |
| 9 | Reductor coal injection pattern (Refer to Figure5): Directly to the centre of reactor $\rightarrow$ Tangentially | 16.89 | 0.43 | 1.71 | 0.40 |
| 10 | Coal size distribution (Refer to Figure 6): Particle diameter ranges: 10-70 μm $\rightarrow$ 10-50 μm | 16.24 | 0.49 | 1.79 | 0.57 |
| 11 | Combustor secondary O$_2$: 70.8 kg/h $\rightarrow$ 53 kg/h Reductor primary O$_2$: 16.28 kg/h $\rightarrow$ 34 kg/h | 16.70 | 0.48 | 1.68 | 2.16 |
| 12 | Combustor coal inlet: 40 kg/h $\rightarrow$ 60 kg/h Reductor coal inlet: 60 kg/h $\rightarrow$ 40 kg/h | 15.89 | 0.39 | 1.66 | -6.31 |
| **Effect of heat loss** | | | | | |
| 13 | Reductor wall boundary condition: Heat loss (2400w/m$^2$) $\rightarrow$ Temperature (1673K) | 32.31 | 0.58 | 1.55 | 79.26 |
| 14 | Heat loss: At combustor wall: 3000 w/m$^2$ $\rightarrow$ 3300 w/m$^2$ At reductor wall: 2400 w/m$^2$ $\rightarrow$ 2640 w/m$^2$ | 16.35 | 0.41 | 1.83 | -3.14 |

The effects of some important model parameters such as latent heat of devolatilization, fraction of heat absorbed by coal particles, absorption coefficient etc. on carbon conversion, syngas production and the product gas temperature are numerically investigated. The predicted results are shown in Figure 2.
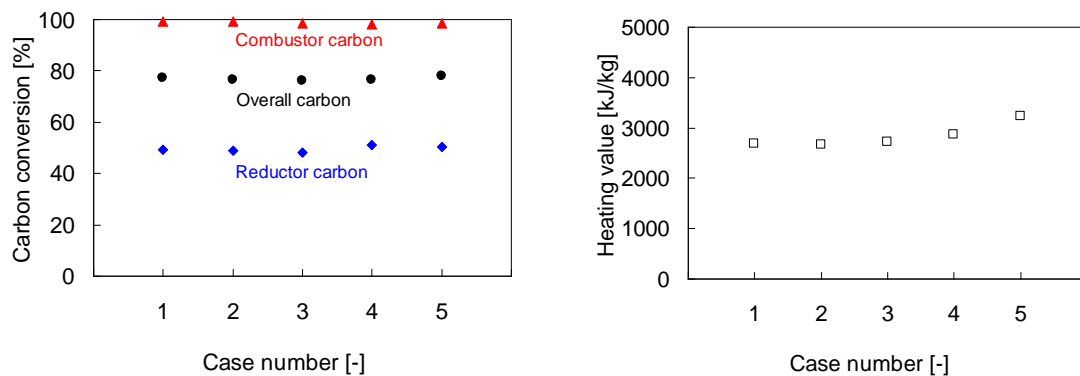


**Figure 2.** Effects of model parameters on carbon conversion and product gas heating value

The latent heat of water present in coal is neglected in the standard case (Case 1). In Case 2, 0.38 MJ/kg-coal of latent heat of water is assumed. This heat is approximately 1.5% of the high heating value of coal (26.40 MJ/kg). A small decrease in outlet gas temperature is found because of heat consumption of water evaporation during devolatilization. Therefore, little changes in carbon conversion and syngas production are obtained. Consequently a small difference in coal heating value will not significantly affect the carbon conversion and syngas production.

The surface reaction consumes or produces energy during the char gasification reactions (R10-R12) in Table 3. The fraction of heat absorbed/released by solid coal particle is represented here as $f_h$. The default value of 1.0 (Case 1) implies that the entire heat of reaction is absorbed/released on the surfaces of particles. To investigate the effect of $f_h$ value on the solid and gas phase, another calculation with a value $f_h = 0.5$ (Case 3) is carried out. There are no significant changes in carbon conversion and syngas heating value found for the two cases. A slight decrease in gas temperature for case 3 is obtained because of consuming energy from gas phase during dominant char-$CO_2$ endothermic reaction (R11).

The effects of radiation parameters on carbon conversion, gas temperature and species concentration are numerically investigated by changing the radiation parameters; scattering coefficient, $\sigma_s$ and absorption coefficient, $a$. $\sigma_s$ is changed from 0 m$^{-1}$ (Case 1) to a value of 1.5 m$^{-1}$ (Case 4). In another calculation, $a$ is increased from a value of 1.5 m$^{-1}$ to 3.0 m$^{-1}$ (Case 5). Carbon conversion, syngas production and product gas temperature increase with increasing $\sigma_s$ and $a$. It is noticeable that increasing $a$ results in a significant change in syngas production. It indicates that endothermic char-$CO_2$ and char-$H_2O$ reactions are enhanced under higher value of $a$. Interestingly, the gas temperature increases although endothermic reactions occur. Since the absorption capacity of $CO_2$ is higher than the other species, $CO_2$ can play an important role to absorb heat from radiation energy under $CO_2/O_2/N_2$ gasification condition.
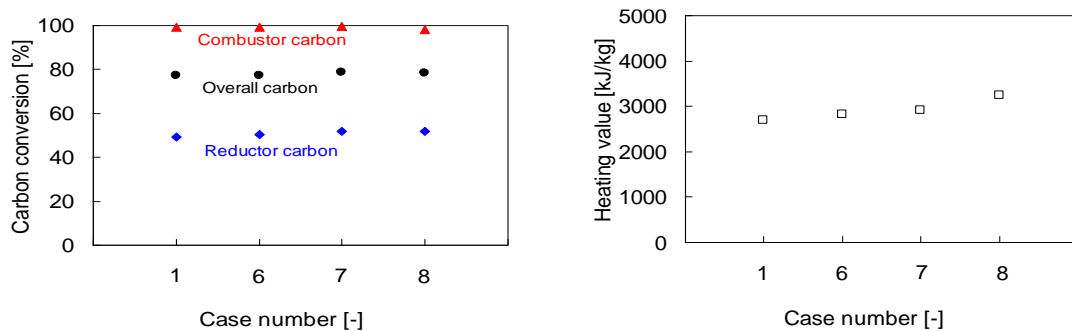


**Figure 3.** Effects of kinetic parameters of char reaction rate on carbon conversion and product gas heating value

### Effects of char kinetic rates

In Cases 6-7, the pre-exponentials for the char-$O_2$ reaction (R-10), the char-$CO_2$ reaction (R-11), and the char-$H_2O$ reaction (R-12) increases respectively by a factor of 10. The calculated carbon conversions and syngas heating values are shown in Figure 3.

It is found that, with increasing the reaction rate of carbon, the reductor carbon conversion increases, while the conversion of combustor carbon remains unchanged. The effect of reaction rate of char-$O_2$ on gas temperature is very small. In contrast, gas temperatures at outlet for Cases 7 and 8 decreases much compared to Case 1 because of enhancing char-$CO_2$ and char-$H_2O$ endothermic reactions. Therefore, by increasing the rate of reaction of char-$CO_2$, it is possible to produce more CO, resulting in an increase in syngas heating value. Since $CO_2$-blown coal gasification operates under $CO_2$-rich condition than the conventional air blown conditions, it can be concluded that $CO_2$-blown coal gasification will be able to produce high heating value gas, resulting in an increase in gasification efficiency. Char-$H_2O$ reaction also plays an important role to increase the syngas heating value. The outlet concentrations increase from 16wt% to 19wt% for CO and 0.46wt% to 0.63wt% for $H_2$.

### Effects of operating conditions

The effects of operating conditions on carbon conversion, syngas heating value and gas temperature are numerically investigated to increase the carbon conversion and syngas heating value without changing the total

gas and coal flow rates. The calculations are carried out by changing the coal injection pattern, coal particle size, coal distribution in the two stages and $O_2$ distribution in the two stages.

In standard case (Case 1), the combustor injectors are placed similar to a tangential firing system to create swirling flow inside the gasifier. While the reductor injectors are directed towards the centre of the gasifier. To investigate the effect of reductor coal injection pattern, the reductor injectors are also placed similar to a tangential firing system. This condition will be referred as Case 9. To make a clear understanding, cross-sectional views of velocity vectors at $z/H_{comb}$=2.2 for Cases 1 and 9 are shown in Figure 4. The results show that reductor coal injection pattern shows a little effect in coal conversions (Figure 5).
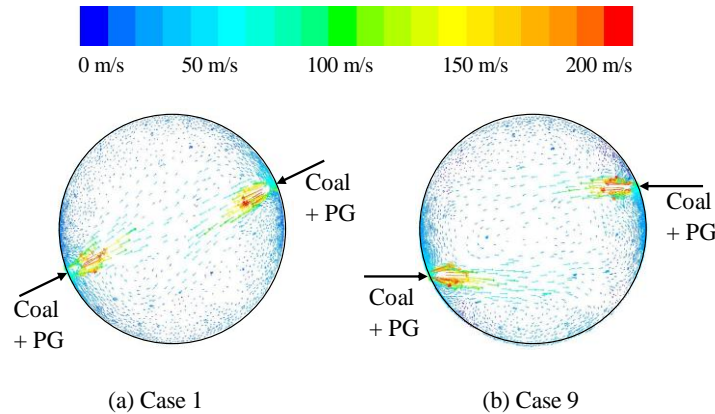


**Figure 4.** Cross-sectional views of velocity vectors colored by velocity magnitude at $z/H_{comb}$=2.2
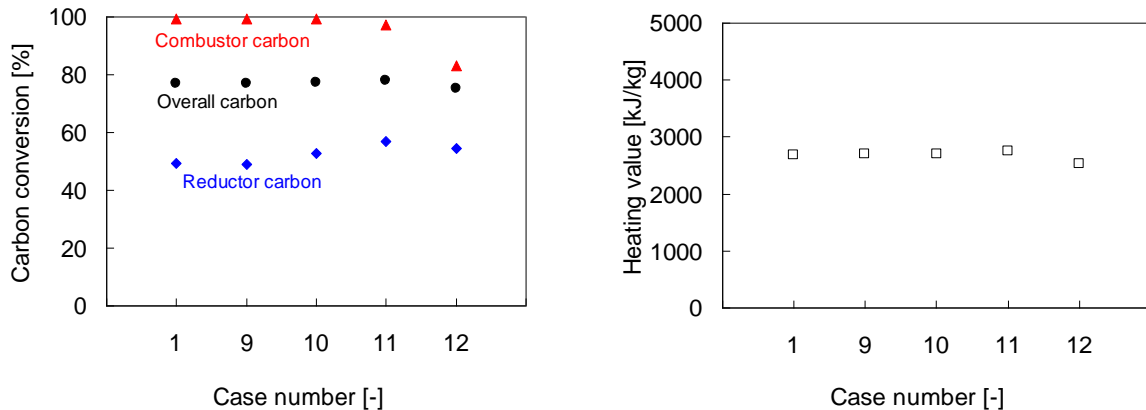


**Figure 5.** Effects of operating conditions on carbon conversion and product gas heating value

To investigate the effect of coal particle diameter on the gas temperature and carbon conversion, a smaller particle size distribution is considered in the calculation. The calculation (case 10) is carried out for coal particles with a mean diameter of 30μm, whose particle size distributions are shown in Figure 6. Little changes in calculated results are observed if the coal particle size distribution is changed from the Case 1 to Case 10 (Figure 5).

The partitioning of $O_2$ between the combustion stage and the reduction stage is investigated by changing the fraction of the total $O_2$ feed into two stages, keeping other parameters fixed. The calculation is carried out under condition where reductor coal primary $N_2$ is replaced by 25wt% of combustor secondary $O_2$ (Case 11). The gas temperatures profiles for Cases 1 and 11 are shown in Figure 7. Case 11 predicts lower gas temperatures in the combustor and higher gas temperatures in the reductor compared with Case 1. A significant gas temperature difference between two cases about 300K is recorded near reductor burner at $z/H_{comb}$=2.2.
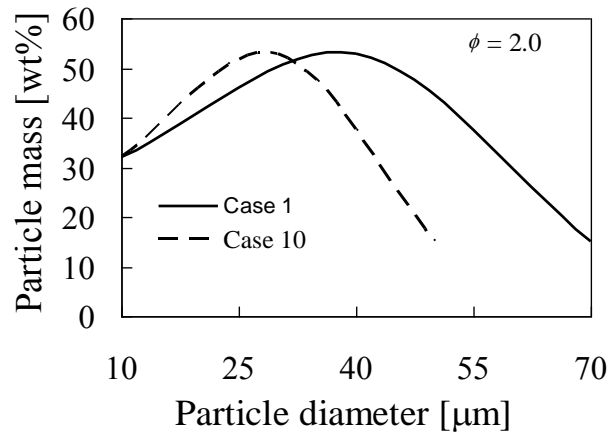
**Figure 6.** Initial coal particle size distributions considered in calculation

This suggests that the partitioning of $O_2$ between two stages plays an important role to control the gas temperature. As shown in Figure 5, carbon conversion in the combustor decreases from 99 wt% to 97 wt% while that in the reductor increases from 49 wt% to 57 wt%. An increase in carbon conversion in the reductor results from an increase in $O_2$ concentration. However, the overall carbon conversion does not change considerably, although the gas temperature in reductor for the case 11 is higher than that for the Case 1. It indicates that the gas temperature is still not sufficient to advance char gasification reactions in the reductor under calculated condition.
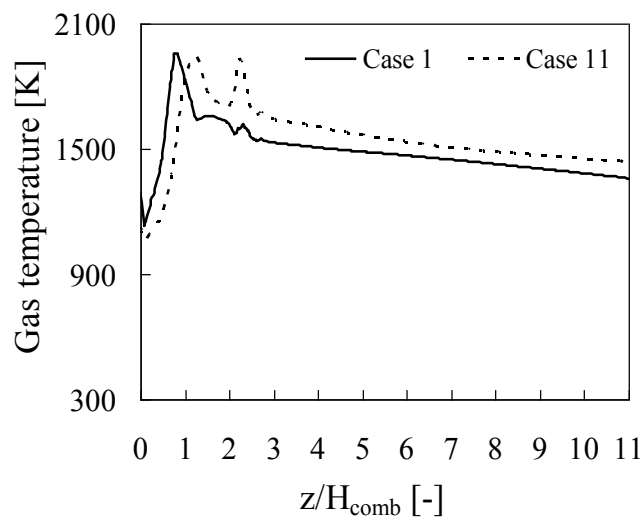


**Figure 7.** Effect of $O_2$ distribution in two stages on gas temperature profiles

The partitioning of coal between the combustion stage and reductor stage is numerically investigated by changing the fraction of the total coal feed rate into the combustor, keeping other parameters fixed. Carbon conversion of combustor coal decreases from 99 wt% to 83 wt% if combustor coal fed increases from 40 kg/h (Case 1) to 60 kg/h (Case 12). The concentration of CO and $H_2$ decrease with a decrease of coal feed rate into the reductor although reductor carbon conversion increases from 49 wt% to 54 wt% while decreasing the reductor coal feed rate from 60 kg/h (Case 1) to 40 kg/h (Case 12). Thus it is not a good reference decreasing the coal feed rate in reductor.

**Effects of heat losses**

By changing various model parameters, kinetic reaction rates and operating conditions (Cases 1 to 12), carbon conversion of redcutor coal is predicted to a maximum value of 57 wt% for Case 12. One common reason

for this limit is due to a low gas temperature in the reductor. For this reason, higher reductor wall temperatures are considered here to ensure higher gas temperatures in the gasifier. Although it is an unusual condition for the real gasifier, this condition is applied to verify what happen if the gasification zone is maintained at higher temperatures condition. A constant reductor wall temperature at 1673K (Case 13) produces higher gas temperatures in the gasifier, resulting in a significant rise in carbon conversion in reductor coal from 49 wt% to 77 wt% as shown in Figure 8. Noticeable outlet concentrations about 32 wt% and 0.58 wt% are obtained for CO and $H_2$, respectively. Therefore, it can be concluded that to obtain higher carbon conversion, it is necessary to increase the gas temperature in the reductor. In another calculation, the effect of heat loss to the reactor wall on carbon conversion and species concentration is numerically studied. The heat loss for Case 14 is increased by 10% of the standard Case 1. An increase in heat loss from wall results a decrease in carbon conversion from 77 wt% to 72 wt% (Figure 8). The gas temperature decreases with increasing heat loss to the wall, while CO and $H_2$ concentration remain unchanged.
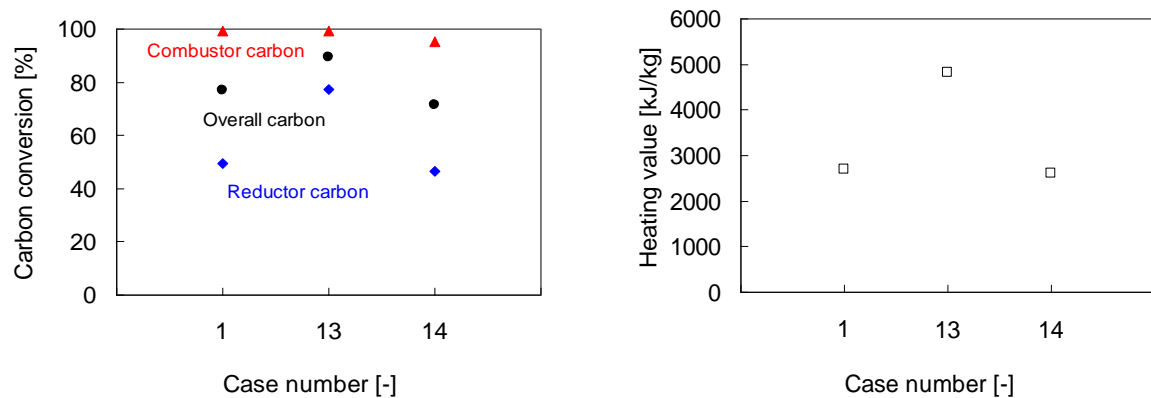


**Figure 8.** Effects of heat losses on carbon conversion and product gas heating value

**Prediction of soot formation**

Referring to the Table 5, it is found that the productions of soot under various changes in model parameters remain unchanged. For case 11, the outlet concentration of soot decreases if the $O_2$ supply in the reductor is increased. The higher gas temperature in the reductor also increases the soot oxidation, resulting in a decrease in soot concentration. The rates of Char-$CO_2$ and char-$H_2O$ reaction also increase at higher temperatures, predicting higher carbon conversion and higher syngas heating value. Table 5 also shows that outlet mass fraction of soot decreases from 1.79 wt% to 1.66 wt% if combustor coal fed increases and reductor coal fed decreases (Case 12). The production of volatiles component $C_6H_6$, which is a precursor of soot formation, increases in the combustor due to increasing coal feed rate. Since combustor is operated at comparatively higher temperatures and under higher $O_2$ concentrations, soot oxidation in the combustor increases, resulting in a decrease in soot concentration. For the case 13, prediction of soot is lowest (1.55 wt%) among all results under calculated conditions. At higher temperature, char-$O_2$ and char-$CO_2$ reaction rates considerably increase and the chance of occurring soot oxidation increases as well.

**CONCLUSIONS**

The numerical simulations of coal gasification in two stage entrained flow gasifier are carried out under various gasification conditions. It is found that the carbon conversions of combustor coal lie in the ranges from 97 wt% to 99 wt% for most of the calculated conditions. While the carbon conversion of reductor coals varies from 45 wt% to 57 wt%. A noticeable change is obtained when the gasification occurs under a high-temperature condition. Remarkable outlet concentrations about 32 wt% and 0.58 wt% are obtained for CO and $H_2$, respectively if high temperature is maintained in the reductor. At a high temperature (1673K), the overall carbon conversion becomes 89 wt%. Soot concentration is found to be decreased if the $O_2$ concentration increases in the gasifier. Therefore, it can be concluded that to get more syngas from $CO_2$-blown coal gasification it is necessary to maintain higher temperatures in the gasifier (reductor).

## ACKNOWLEDGMENTS

## NOMENCLATURE

| | |
|---|---|
| $A$ | Absorption Coefficient [m$^{-1}$] |
| $a_p$ | Equivalent Absorption Coefficient [m$^{-1}$] |
| $A$ | Surface Area [m$^2$] |
| $A_f$ | Pre-exponential Factor [kg/m$^2$·s·Pa], [s$^{-1}$] |
| $A_R$ | Magnussen Constant for Reactants [-] |
| $B_P$ | Magnussen Constant for Products [-] |
| $c_p$ | Specific Heat of Gas [J/kg·K] |
| $C_P$ | Specific Heat of Coal Particle [J/kg·K] |
| $d$ | Diameter [m] |
| $\overline{d}_p$ | Mean Diameter of Coal Particle [m] |
| $D_k$ | Diffusion Coefficient in $k$th Reaction [m$^2$/s] |
| $E$ | Energy [J] |
| $E_p$ | Equivalent Emission of Coal Particles [W/m$^3$] |
| $f_p$ | Particle Scattering Factor [-] |
| $f_w$ | Fraction of Water Present in Coal Particles [-] |
| $f_h$ | Fraction of Heat Absorbed by Coal Particles [-] |
| $g$ | Gravitational Acceleration [m/s$^2$] |
| $h$ | Heat Transfer Coefficient [W/m$^2$·K] |
| $H$ | Enthalpy [J/kg] |
| $H_{comb}$ | Height of Combustor [m] |
| $I$ | Number of Species [-] |
| $I_{rad}$ | Radiation Intensity [W/m$^2$] |
| $I_t$ | Turbulent Intensity [-] |
| $J_i$ | Mass Flux of Species $i$ [kg/m$^2$·s] |
| $k$ | Turbulent Kinetic Energy [m$^2$/s$^2$] |
| $k_g$ | Thermal Conductivity of Gas [W/m·K] |
| $k_{kin}$ | Reaction Rate Constant [unit vary] |
| $K$ | Number of Reactions [-] |
| $L$ | Latent Heat of Water Present in Coal [J/kg-coal] |
| $m$ | Mass [kg] |
| $m_p$ | Mass of Coal Particle [kg] |
| $M_i$ | Molecular Weight of Species $i$ [kg/kmol] |
| $n$ | Spread Parameter [-] |
| $N$ | Order of Reaction [-] |
| Nu | Nusselt Number [-] |
| $p$ | Pressure [Pa] |
| Pr | Prandtl Number [-] |
| $q$ | Heat Flux [J/m$^2$] |
| $\vec{r}$ | Position Vector [m] |
| $R$ | Universal Gas Constant (8.314×10$^3$) [J/kmol·K] |
| $R_i$ | Source of Chemical Species $i$ due to Reaction [kg/m$^3$·s] |
| $\hat{R}_{i,k}^{(A)}$ | Rate of Production [Arrhenius] of species $i$ in $k$th Reaction [kmol/m$^3$·s] |
| $\hat{R}_{i,k}^{(R)}$ | Rate of Production [Eddy Dissipation] of Reactant $i$ in $k$th Reaction [kmol/m$^3$·s] |
| $\hat{R}_{i,k}^{(P)}$ | Rate of Production [Eddy Dissipation] of Product $i$ in $k$th Reaction [kmol/m$^3$·s] |
| $\overline{R}_k$ | Rate of Particle Surface Species Depletion in $k$th Reaction [kg/s] |
| $\tilde{R}_k$ | Rate of Particle Surface Species Reaction per unit Area in $k$th Reaction [kg/m$^2$·s] |
| $Re_d$ | Reynolds Number Based on the Particle Diameter [-] |
| $s$ | Path Length [m] |

| | |
|---|---|
| $\vec{s}$ | Direction Vector [m] |
| $S$ | Entropy [J/kmol·K] |
| $S_m$ | Rate of Mass Added from Coal Particle [kg/m²·s] |
| $S_{h,reac}$ | Source of Heat due to Reaction [W/m²·s] |
| $Sc_t$ | Turbulent Schmidt Number [-] |
| $t$ | Time [s] |
| $T$ | Temperature [K] |
| $u, v, w$ | Velocity Magnitude [m/s] |
| $\vec{v}$ | Velocity Vector [m/s] |
| $\overline{u_i}$ | Mean Velocity Component |
| $u_i^{/}$ | Fluctuating Velocity Component |
| $V$ | Volume [m³] |
| $X_i$ | Molar Concentration of Species $i$ [kmol/m³] |
| $y^+$ | Dimensionless Distance [-] |
| $Y_i$ | Mass Fraction of Species $i$ [-] |
| $z$ | Height of Reactor [m] |

**Greek letters**

| | |
|---|---|
| $\alpha_1$ | Yield Parameter for First Step Devolatilization [-] |
| $\alpha_2$ | Yield Parameter for Second Step Devolatilization [-] |
| $\varepsilon$ | Turbulent Dissipation rate [m²/s³] |
| $\varepsilon_p$ | Emissivity of Coal Particle [-] |
| $\eta$ | Effectiveness Factor [-] |
| $\eta', \eta''$ | Rate Exponent for Reactants, Products [-] |
| $v', v''$ | Stochiometric Coefficient for Reactants, Products [-] |
| $\theta_R$ | Radiation Temperature [K] |
| $\mu$ | Dynamic Viscosity [Pa·s] |
| $\mu_t$ | Turbulent Viscosity [Pa·s] |
| $\rho$ | Density [kg/m³] |
| $\sigma$ | Stefan-Boltzmann Constant (5.669×10⁻⁸ ) [W/m²·K⁴] |
| $\sigma_k$ | Turbulent Prandtl Number for $k$ [-] |
| $\sigma_\varepsilon$ | Turbulent Prandtl Number for $\varepsilon$ [-] |
| $\sigma_s$ | Scattering Coefficient [m⁻¹] |
| $\sigma_p$ | Equivalent Particle Scattering Factor [m⁻¹] |
| $\Omega$ | Solid Angle [degree] |

**Subscripts**

| | |
|---|---|
| a | Ash |
| ac | Activation |
| b | Backward |
| f | Forward |
| i | Species |
| h | Heat |
| m | Mass |
| P | Product Species |
| p | Particles |
| R | Reactant Species |
| rad | Radiation |
| t | Turbulent |
| 0 | Initial Stage |

## REFERENCES

[1] Ministry of Economy, Trade and Industry, Energy in Japan 2010, Japan 13–14 (2010)

[2] Luan, Y.T., Chyou, Y.P., Wang, T.: Numerical analysis of gasification performance via finite-rate model in a cross-type twostage gasifier. Int. J. Heat Mass Transf. 57, 558–566 (2013)

[3] Chen, C., Masayuki, H., Toshinori, K.: Numerical simulation of entrained flow coal gasifiers Part I: modeling of coal gasification in an entrained flow gasifier. Chem. Eng. Sci. 55, 3861-3874 (2000)

[4] Chen, C., Masayuki, H., Toshinori, K.: Numerical simulation of entrained flow coal gasifiers Part II: effects of operating conditions on gasifier performance. Chem. Eng. Sci. 55, 3875-3883 (2000)

[5] Silaen, A., Wang, T.: Effect of turbulence models on gasification simulation. Proceedings of the 25th International Pittsburgh Coal-Gen Conference, Pittsburgh, Pennsylvania, September (2008)

[6] Silaen, A., Wang, T.: Effects of fuel injection angles on performance of a two stage coal gasifier. Proceedings of the 23rd Pittsburgh Coal Conference, Pittsburgh, Pennsylvania, September (2006)

[7] Silaen, A., Wang, T.: Effect of turbulence and devolatilization models on coal gasification simulation in an entrained-flow gasifier. Int. J. Heat Mass Transf. 53, 2074–2091 (2010)

[8] Alam, M.S., Agung, T.W., Nakaso, K., Fukai J.: Study on coal gasification with soot formation in two-stage entrained-flow gasifier. Int. J. Energy Environ. Eng. 6(3), 255-265 (2015)

[9] National Institute of Standards and Technology (NIST) chemistry web book.

[10] Hara, S., Oki, Y., Kajitani, S., Watanabe, H., Umemoto, S.: Examination of Gasification Characteristics of Pressurized Two-stage Entrained-flow Coal Gasifier - Influence of Oxygen Concentration in Gasifying Agent. CRIEPI Energy Engineering Research Laboratory Report No. M08019 (2009)

[11] Ansys Fluent 12.0 User's Guide, Ansys Inc., 2009

[12] Kidoguchi, K., Kajitani, S., Oki, Y., Umemoto, S., Umetsu, H., Hamada, H., Hara S.: Evaluation of CO2 Enriched Gasification Characteristics Using 3t/d Bench Scale Coal Gasifier - Influence of CO2 Concentration in Gasifying Agent. CRIEPI Energy Engineering Research Laboratory Report No. M11019 (2012)

[13] Kobayashi, H., Howard, J.B., Sarofim, A.F.: Coal Devolatilization at High Temperatures. Symposium (International) on Combustion. 16, 411-425 (1977)

[14] Hashimoto, N., Kurose, R., Shirai, H.: Numerical simulation of pulverized coal jet flame employing the TDP model. Fuel 97, 277-287 (2012)

[15] Watanabe, H., Otaka, M.: Numerical simulation of coal gasification in entrained-flow coal gasifier. Fuel 85, 1935-1943 (2006)

[16] Wijayanta, A.T., Alam, M.S., Nakaso, K., Fukai, J.: Numerical investigation on combustion of coal volatiles under various O2/CO2 mixtures using a detailed mechanism with soot formation. Fuel 93, 670-676 (2012)

[17] Massachusetts Ins. of Tech., Combustion Research Website (http://web.mit.edu)

[18] Kazakov, A., Wang, H., Frenklach, M.: Detailed modeling of soot formation in laminar premixed ethylene flames at a pressure of 10 bar. Combust. Flame 100, 111-120 (1995)